Electrostatic Influence of PsaC Protein Binding to the PsaA/PsaB Heterodimer in Photosystem I

Hiroshi Ishikita,* Dietmar Stehlik,† John H. Golbeck,‡ and Ernst-Walter Knapp*

*Institute of Chemistry and Biochemistry, Department of Biology, Chemistry, and Pharmacy, and †Department of Physics, Free University of Berlin, D-14195 Berlin, Germany; and ‡Department of Biochemistry and Molecular Biology and Department of Chemistry, The Pennsylvania State University, University Park, Pennsylvania 16802

ABSTRACT The absence of the PsaC subunit in the photosystem I (PSI) complex (native PSI complex) by mutagenesis or chemical manipulation yields a PSI core (P700-F_X core) that also lacks subunits PsaD and PsaE and the two iron-sulfur clusters F_A and F_B, which constitute an integral part of PsaC. In this P700-F_X core, the redox potentials (E_m) of the two quinones $A_{1A/B}$ and the iron-sulfur cluster F_X as well as the corresponding protonation patterns are investigated by evaluating the electrostatic energies from the solution of the linearized Poisson-Boltzmann equation. The B-side specific Asp-B558 changes its protonation state significantly upon isolating the P700-F_X core, being mainly protonated in the native PSI complex but ionized in the P700-F_X core. In the P700-F_X core, $E_m(A_{1A/B})$ remains practically unchanged, whereas $E_m(F_X)$ is upshifted by 42 mV. With these calculated E_m values, the electron transfer rate from A_1 to F_X in the P700-F_X core is estimated to be slightly faster on the A_{1A} side than that of the wild type, which is consistent with kinetic measurements.

INTRODUCTION

The x-ray crystal structure of Photosystem I (PSI) from *Thermosynechococcus elongatus* at 2.5 Å resolution (1) solved the riddle of the microscopic structure of this protein-pigment complex located in the thylakoid membrane. The central part of PSI is composed of two homologous membrane integral subunits, PsaA and PsaB (Fig. 1 *A*). The two homologous chains harbor as redox-active cofactors a dimer of chlorophyll *a* (Chl*a*, P700), two accessory Chl*a*, (A_{-1}), two additional distant Chl*a* (A_0), two phylloquinones (phyllo-Q, A_1), and one iron-sulfur cluster (F_X). The stromal extrinsic subunit PsaC contains two additional iron-sulfur clusters (F_A and F_B). Similarly to bacterial photosynthetic reaction centers (RC), these six Chl*a* and two phyllo-Q cofactors are arranged in two branches (A and B) in pseudo C_2 symmetry with the rotation axis passing through P700 and F_X. The axially located P700 and F_X, in turn, are connected by the two chains of redox-active cofactors $A_{-1A/B}$, $A_{0A/B}$, and $A_{1A/B}$.

Subunit PsaC is largely similar to ferredoxins that contain two Fe_4S_4 clusters. To test the functional role of this subunit, a PSI mutant lacking subunit PsaC (P700-F_X core) is studied in this work. A consequence of the P700-F_X core preparation is not only the absence of PsaC, which contains the two iron-sulfur clusters F_A and F_B, but also the lack of PsaD and PsaE; these two subunits are in close contact with PsaC and bind to PsaA/PsaB only after PsaC is bound. A P700-F_X core can be generated either chemically i), by urea treatment (urea-treated PSI) (2–5) or genetically in two ways by deleting ii), the *psaC* gene (*psaC*$^-$ PSI) (4,6), or iii), the *rub*A gene (*rub*A$^-$ PSI) (7,8). The latter leads to a P700-F_X core in which F_X is initially absent but can be later reconstituted. If not otherwise specified, we name all three differently generated incomplete PSI protein complexes ''P700-F_X cores'' in this study. Despite the deletion of the subunit PsaC in the neighborhood of F_X, the measured electron transfer (ET) rate from A_1 to F_X remains essentially unchanged (180 ns by ultraviolet-visible (UV-VIS) spectroscopy (9) or 190 ns by electron paramagnetic resonance (EPR) (10) in urea-treated PSI) relative to the native PSI complex, where the corresponding time constant was between 206 ns and 355 ns (11–16).

Here, we present the calculated $E_m(A_{1A/B})$ values for the P700-F_X core as we presented in our previous work for the native PSI complex (17). The shift of calculated $E_m(F_X)$ in the P700-F_X core versus the corresponding value in the native PSI complex is also correlated with corresponding ET rates measured on P700-F_X cores generated by urea treating of PSI (9,10). To investigate the electrostatic binding interaction between the PSI subunits, we present the calculated pKa values for residues in the binding interface or, if needed, we constrain the protonation probability of specific residues whose charge state was considered to be significant for PsaC binding (4,18) and monitor the resulting changes in protonation pattern. With this simple method, we obtain information on the electrostatic interaction of binding the PsaC subunit to the PsaA/PsaB heterodimer.

A key question for PSI research is the role of partial negative charges on the E_m of the cofactors involved in light-induced charge separation and thus in control of functional properties. In particular, the nominal negative charge of the Fe_4S_4 clusters can directly contribute to the E_m shift of the cofactors that precede it in the ET chain, such as A_1, as

Submitted July 1, 2005, and accepted for publication October 7, 2005.

Address reprint requests to E. W. Knapp, Tel.: 49-30-8385-4387; Fax: 49-30-8385-6921; E-mail: knapp@chemie.fu-berlin.de.

Hiroshi Ishikita's present address is Dept. of Chemistry, The Pennsylvania State University, 104 Chemistry Building, University Park, PA 16802.

0006-3495/06/02/1081/09 $2.00

doi: 10.1529/biophysj.105.069781

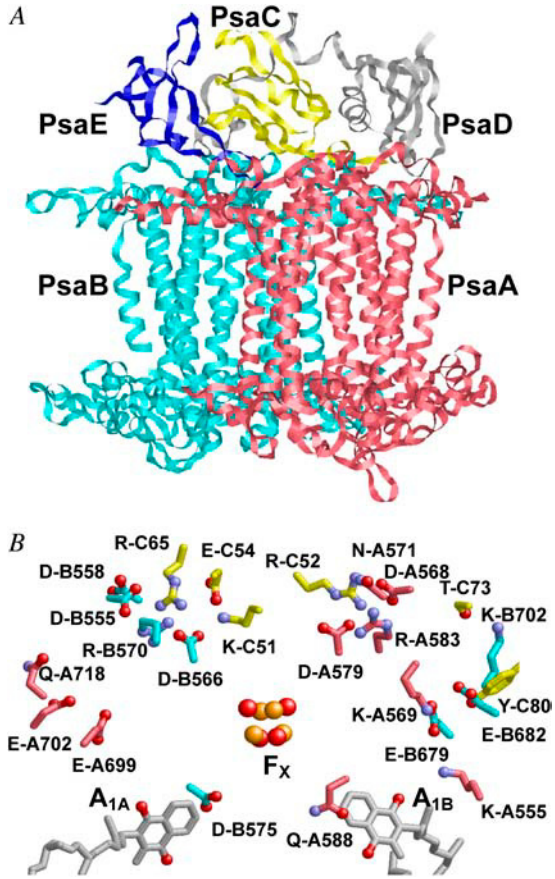

FIGURE 1 (*A*) Location of PsaA, PsaB, PsaC, PsaD, and PsaE subunits (displayed in *pink*, *cyan*, *yellow*, *gray*, and *blue*, respectively). (*B*) Selected residues of the interface of PsaC binding to the PsaA/PsaB heterodimer. Residues discussed in the text and Table 1 are displayed with ball and stick, in red (PsaA), blue (PsaB), and yellow (PsaC).

recently demonstrated computationally (17) and experimentally (19,20). Selective removal of particular Fe_4S_4 clusters is a feasible experimental approach, which is pursued here computationally.

MATERIALS AND METHODS

Coordinates

For our computations, we used the crystal structure of trimeric PSI from *T. elongatus* at 2.5 Å resolution (Protein Data Bank; 1JB0) (1).

The crystal structure of the P700-F_X core is yet not available. In the model of the P700-F_X core, the subunits PsaC, PsaD, and PsaE were removed together with the iron-sulfur cofactors F_A and F_B, which are embedded in PsaC. It has been established in vitro that PsaC can be rebound to the P700-F_X core without the need for ATP hydrolysis and without the need of chaperones (6,21). It has also been suggested from urea-treated PSI that the P700-F_X core represents the intact PSI core and retains >90% of F_X with little deterioration of the RC (2), because the binding contacts between PsaC and the PsaA/PsaB heterodimer are mainly electrostatic in nature (1,18,22). EPR data show that structural and kinetic properties of the A_1 site remain identical within experimental accuracy for the P700-F_X core and the native complete PSI complex (10). The structural model used for the P700-F_X core in this study is, therefore, the best starting point and in part justified by experimental evidence.

For both the P700-F_X core and the native PSI complex, the atomic coordinates were treated as in previous work (17). In the crystal structure, hydrogen atom positions were energetically optimized with CHARMM (23). During this procedure the positions of all nonhydrogen atoms were fixed; all titratable groups were kept in their standard protonation state, i.e., acidic groups were ionized and basic groups were protonated. The six Chl*a* and the two phyllo-Q were kept in the oxidized neutral charge state. Analogous to the wild-type PSI, one specific crystal water (HOH-37) was also considered for the P700-F_X core (17). This water molecule forms an H bond with one of the acidic oxygens of Asp-B575 that was found to change its protonation state coupled with the redox states of $A_{1A/B}$ as discussed later. If not otherwise stated, the results refer to computations that include this crystal water.

Atomic partial charges

Atomic partial charges of the amino acids were adopted from the all-atom CHARMM22 (24) parameter set. The charges of acidic oxygens were both increased symmetrically by +0.5 unit charges to account implicitly for the presence of the proton. Similarly, instead of removing a proton in the deprotonated state, the charges of all protons of the basic groups of arginine and lysine were diminished symmetrically by a total unit charge. For residues whose protonation states are not available in the CHARMM22 parameter set, appropriate charges were computed (25). For the cofactors, the same atomic charges as in our previous computation (17) were used. We considered F_X, F_A, and F_B in the oxidized charge state $[Fe_4S_4(SCH_3)_4]^{2-}$ for the native PSI complex (26). To obtain the shift of $E_m(F_X)$ between the native PSI and the P700-F_X core, we considered $[Fe_4S_4(SCH_3)_4]^{2-/3-}$ for the oxidized/reduced state of F_X ($F_X^{0/-}$). As in previous computations (17), a positive unit charge was located on the B-branch Chl*a* of the P700 dimer ($P700_B$), according to electron nuclear double resonance (ENDOR) and electron spin echo envelope modulation (ESEEM) studies (27–30).

Computation of protonation pattern and redox potential

Our computation is based on the electrostatic continuum model by solving the linearized Poisson-Boltzmann (LPB) equation with the program MEAD (31). The protonation patterns were sampled by a Monte Carlo (MC) method with our own program Karlsberg (32). The dielectric constant was set to $\varepsilon_P = 4$ inside the protein and $\varepsilon_W = 80$ for water as done in previous computations (for instance, Ishikita and Knapp (17)). All computations refer to pH 7.0 at 300 K and an ionic strength of 100 mM. The LPB equation was solved using a three-step grid-focusing procedure with 2.5 Å, 1.0 Å, and 0.3 Å resolution. The MC sampling yields the probabilities $[A_{ox}]$ and $[A_{red}]$ of the redox states of compound *A*.

The E_m was calculated from the Nernst equation. To minimize the statistical error in evaluating the E_m, a bias potential was applied to obtain an equal amount of both redox states ($[A_{ox}] = [A_{red}]$), yielding the value of the bias potential as the resulting E_m. For convenience, the computed E_m are given with mV accuracy, without implying that the last digit is significant. To obtain the absolute value of E_m in the protein, we calculated the electrostatic energy difference between the two redox states of phyllo-Q in the protein and a reference model system where the experimental redox potential is known. The shift of the E_m in the protein relative to the reference system was added to this experimental value. As a reference model system, we used the E_m(phyllo-Q) of −463 mV versus NHE (normal hydrogen electrode) for one-electron reduction in DMF solution (33) as was done in the previous study (17).

We can calculate pKa values for titratable residues using two different pKa definitions. In a straightforward approach, a titratable residue is biased by an individual energy term to be 50% protonated, whereas the protonation

states of the other titratable residues are fully relaxed at a fixed pH (pH 7 in this study). This bias energy can be used to define the pKa of this residue (Henderson-Hasselbalch pKa). This pKa describes how much energy is needed to change the protonation state of this residue in its protein environment where the protonation pattern changes locally by equilibration due to the charge change of this residue without involving changes of solvent pH. This pKa definition is, for instance, useful to describe the energetics of the adiabatic proton transfer processes between different titratable groups. The protonation dependence of the considered titratable residue obeys the Henderson-Hasselbalch equation (equivalent to the Nernst equation for a redox-active group) as a function of the bias energy.

Another approach to determine pKa values is to calculate it from the protonation pattern of all titratable residues as a function of solvent pH for a large pH range. Here, the pKa of the titratable residue under consideration can be defined as the pH value where this residue is to 50% protonated [effective pKa]. This is a more common pKa definition and corresponds to the conditions where pKa values of titratable groups in proteins are determined experimentally. When the molecular system contains only a single or several noninteracting titratable groups, the same pKa values are computed for both definitions.

In a region rich in titratable residues, it is often hard to give a specific single value for the effective pKa if one observes only a moderate protonation change over a wider pH range. In this study, we calculated pKa values as Henderson-Hasselbalch pKa at pH 7.0 as in previous studies (34,35), whereas protonation probabilities are computed by coupling solvent pH at pH 7 to all titratable residues and not by using a bias energy term. Protonation probabilities obtained in this way qualitatively relate to the pKa definition effective pKa. But, there is no quantitative correspondence between these protonation probabilities and pKa derived from the simple Henderson-Hasselbalch relation because of possible strong electrostatic coupling between different titratable residues (for further discussions about the difference between the Henderson-Hasselbalch and the effective pKa, see Supplemental discussion). Note that we do not consider possible structural changes of a protein upon pH changes. Such structural changes may occur more prominently in protein regions containing clusters of titratable residues.

Estimation of the ET rate

We estimated the ET rate from A_1 to F_X based on the values of $E_m(A_1)$ and $E_m(F_X)$ by evaluating the following empirical rate expressions (36). They describe ET processes at $T = 300$ K, which are downhill in energy (exergonic)

$$k_{T=300\,K}^{\text{exergonic ET}} = 10^{(13-0.6(\mathbf{R}-3.6)-3.1(-|\Delta\mathbf{G}|+\boldsymbol{\lambda})^2/\boldsymbol{\lambda})}, \quad (1)$$

or uphill in energy (endergonic)

$$k_{T=300\,K}^{\text{endergonic ET}} = k_{T=300\,K}^{\text{exergonic ET}} 10^{3.1|\Delta\mathbf{G}|/0.06}, \quad (2)$$

where R (>3.6 Å) is the edge-to-edge distance, ΔG the E_m difference of the participating electron donor and acceptor groups, and λ the reorganization energy. In these rate expressions, the energy parameters (ΔG and λ) are given in units of eV and the distances (R) in units of Å. The edge-to-edge distance R of donor (A_1) and acceptor group (F_X) is $R = 6.8$ Å, identical in both A_{1A} and A_{1B} sides, as taken from the crystal structure (1).

RESULTS AND DISCUSSION

Role of the specific protonation pattern in the P700-F_X cores

Redox states $A_{1B}^{0/-}$ influencing Glu-B682

Fourier transform infrared (FTIR) spectroscopic studies indicated that one glutamate was perturbed upon formation of A_1^- in wild-type PSI. As possible candidates, glutamates A699, A702, B679, and B682 were proposed (37). The pairs of symmetry-related glutamates Glu-A702/Glu-B682 and Glu-A699/Glu-B679 are located in equivalent positions in the A- and B-branches, respectively. In our previous study of the wild-type PSI, we found that among these glutamates only Glu-B682 showed a small but notable increase in protonation (protonation state of 0.15 H^+) with the formation of A_{1B}^- (17), whereas this residue was fully ionized in the A_{1B}^0 state. Concerning A_{1A}^0 and these glutamates, the pKa calculated for Glu-B-682 is significantly higher for both redox states than those of the other three glutamates (Table 1). A comparison between the symmetry-related pairs of glutamates reveals that Glu-A699 and Glu-B679 possess similar pKa values, whereas the pKa of Glu-A702 and Glu-B682 show a significant difference. The latter indicates that the electrostatic environment of these symmetry-related glutamates

TABLE 1 Calculated pKa values of residues for the native PSI complex and the P700-F_X core in the P_B^+ state

Residues of PsaA	Redox state*	Native PSI	P700-F_X core	Residues of PsaB	Redox state*	Native PSI	P700-F_X core
Asp-A568		3.9	4.7	Asp-B555		4.1	5.6
(Asn-A571)†				Asp-B558		8.5	5.7
Asp-A579		−0.3	2.0	Asp-B566		−4.8	3.3
Arg-A583		22.3	13.6	Arg-B570		21.3	15.5
(Gln-A588)†				Asp-B575		5.2	4.7
					A_{1A}^-	8.7	7.9
					A_{1B}^-	7.2	6.9
					F_X^-	9.2	8.2
Glu-A699		−2.6	−2.4	Glu-B679		−4.2	−4.3
	A_{1A}^-	−2.7	−2.4		A_{1B}^-	−3.8	−3.9
Glu-A702		−1.3	2.6	Glu-B682		4.7	5.2
	A_{1A}^-	−1.3	2.8		A_{1B}^-	6.2	5.9
(Gln-A718)†				Lys-B702		16.4	10.0

*If no redox state is indicated, all redox active cofactors are in the neutral charge state except for P_B^+.
†Nontitratable residue in PsaA, which is symmetry related to a titratable residue in PsaB.

belonging to the A- and B-branches is asymmetric. Related to this difference, we found an asymmetry of the corresponding protein conformations in the immediate vicinity. The backbone nitrogen of Lys-B551 is at a distance of only 2.9 Å from the acidic oxygen of Glu-A702, stabilizing its ionized state by this H bond and thus rendering Glu-A702 very acidic. The symmetry-related residue to Lys-B551 is Arg-A564. In contrast to Lys-B551 the backbone nitrogen of Arg-A564 is at a distance of 3.9 Å from the acidic oxygen of Glu-B682, which is too far to barely form an H bond. As a consequence the pKa of Glu-B682 is calculated to be significantly higher than that of Glu-A702 (Table 1), the former being close to the reference value of 4.4 in aqueous solution.

In the P700-F_X core environment around A_{1B}^-, Glu-B682 is slightly more ionized (protonation 0.08 H^+) than in the native PSI complex. In the P700-F_X core, the quartet of glutamates appears on the protein surface, stabilizing the deprotonated state. At the same time, the solvent exposure, especially of Glu-B682, shields the charge influence from A_{1B}, thus reducing the pKa difference between the two redox states $A_{1B}^{0/-}$ from 1.5 in the native PSI complex to 0.7 in the P700-F_X core (Table 1).

Asp-B575 influenced by the redox states $A_{1A/B}^{0/-}$ and $F_X^{0/-}$

In the native PSI complex, Asp-B575 in the neighborhood of A_{1A} changes its protonation state in response to the formation of $A_{1A/B}^-$ (17). The symmetry counterpart of Asp-B575 in PsaB is the nontitratable residue Gln-A588 in PsaA. This Gln-A558/Asp-B575 pair is highly conserved from cyanobacteria to higher plants. One of the acidic oxygens of Asp-B575 is H-bonded to the crystal water HOH-37 as a part of a larger water network located between the cofactors $A_{1A/B}$ and F_X, which apparently displays a PsaA/PsaB asymmetry (1). In the P700-F_X core, upon formation of A_{1A}^- and A_{1B}^- the protonation probabilities of Asp-B575 are 0.89 H^+ and 0.27 H^+, respectively, whereas this residue is fully ionized in the A_{1A}^0/A_{1B}^0 state. The similarity of the Asp-B575 protonation state between the P700-F_X core and the native PSI complex (0.85 H^+ for A_{1A}^- and 0.17 H^+ for A_{1B}^- in the latter (17)) indicates that Asp-B575 is electrostatically also buried in the P700-F_X core as deduced also from the crystal structure (1) for the native PSI complex. Hence, it is well shielded from the stromal surface of the PsaA/PsaB complex such that the influence of PsaC on Asp-B575 is small. As will be discussed later, the small decrease of protonation state of Asp-B575 by 0.10 H^+ for A_{1B}^- relative to the native PSI complex can partially contribute to the upshift of $E_m(A_{1B})$ in the P700-F_X core.

In this study on the P700-F_X core, we additionally found that upon formation of F_X^-, Asp-B575 is mostly protonated in both the native PSI complex and the P700-F_X core (protonation states of 0.95 H^+ and 0.94 H^+, respectively). Indeed, the calculated pKa values for Asp-B575 are 9.4 (8.6) in the F_X^- state, followed by 8.9 (8.3) in the A_{1A}^- state, 7.4 (7.0) in the A_{1B}^- state, and 5.4 (5.1) in the neutral state (A_{1A}^0/A_{1B}^0) of the native PSI complex (P700-F_X core) (Table 1).

Analysis of protonation pattern changes on PsaC binding

Arg-C65

Arg-C65 participates in the H-bond network surrounding HOH-22. Its influence on the protonation pattern of titratable residues in its neighborhood is investigated by constraining it to be in the deprotonated charge state. In response to the deprotonation of Arg-C65, a dramatic change in protonation pattern is induced at Asp-B555 (0.00 H^+ → 1.00 H^+), Asp-B558 (0.97 H^+ → 0.07 H^+), and Glu-C54 (0.00 H^+ → 0.23 H^+) (Table 2). Arg-C65 is involved in the specificity of binding between PsaB and PsaC by forming at pH 7.0 simultaneously strong salt bridges with Asp-B555 (N_{Arg}–O_{Asp} distance 3.0 Å) and Asp-B566 (N_{Arg}–O_{Asp} distance 2.6 Å) (see also Table 3 of Antonkine et al. (18)). In contrast to Asp-B555, Asp-B566 is always ionized.

Lys-C51 and Arg-C52

Two double mutants, K(C51)S/R(C52)D and K(C51)S/R(C52)A, which did not prevent association of PsaC with PsaA and PsaB to the PSI complex, were originally constructed to test the influence of these two basic residues Lys-C51 and Arg-C52 on $E_m(F_{A/B})$ (38) (see also Golbeck (4)). On the other hand, from analysis of the crystal structure (18) it is evident that Lys-C51 forms salt bridges with Asp-B566 and Glu-C54, whereas Arg-C52 forms salt bridges with Asp-A568 and Asp-A579 (Fig. 1 *B*). Hence, although these central salt bridges that stabilize the association between PsaC and PsaA/PsaB are lost in those double mutants, there still exist the salt bridges between Arg-C65 and Asp-B555/Asp-B566, which may be sufficient to guarantee binding of a functional PsaC (4).

To investigate the influence of the basic residues Lys-C51 and Arg-C52 on the acidic residues serving as salt bridge partners, we force each of the two basic residues individually in the deprotonated state. Hereby, Asp-A568 becomes protonated upon deprotonation of Arg-C52, whereas all other acidic residues do not change their protonation state (including Asp-A579) and remain ionized (Table 2). This may suggest that Arg-C52 couples more strongly with Asp-A568 (N_{Arg}–O_{Asp} distances of 2.8 Å and 3.2 Å) than with Asp-A579 (N_{Arg}–O_{Asp} distances 2.8 Å and 3.1 Å), although

TABLE 2 Changes in protonation pattern with forced deprotonation of residues Lys-C51, Arg-C52, and Arg-C65 in PsaC

Deprotonated residue*	Affected residues	Protonation probability change
Lys-C51	Glu-C54	0.00 → 1.00
Arg-C52	Asp-A568	0.00 → 1.00
Arg-C65	Asp-B555	0.00 → 1.00
	Asp-B558	0.97 → 0.07
	Glu-C54	0.00 → 0.23

*Protonation state of the residue was forced to change from 1.0 H^+ to 0.0 H^+ (deprotonation).

the N–O distances in the two salt bridges are practically identical. The strongly ionized state for Asp-A579 is due to the proximity of Arg-A583 (closest N_{Arg}–O_{Asp} distance 3.0 Å). The formation of salt bridges between them renders the pKa for Asp-A579/Arg-A583 extremely low/high, resulting in a pKa for Asp-A579 by 4 pH units lower than that of Asp-A568 (Table 1).

Enforced deprotonation of Lys-C51 results in protonation of the salt bridge partner Glu-C54 (Table 2), whereas no change of protonation state is observed for the other salt bridge partner, Asp-B566. This may be due to the simultaneous involvement of Asp-B566 in an intermolecular salt bridge with Lys-C51 and Arg-C65 (Fig. 1 *B*). In addition, Asp-B566 has an intramolecular salt bridge partner, Arg-B570 (closest $N_{Arg} - O_{Asp}$ distance of 2.7 Å). This strong intramolecular salt bridge stabilizes the ionized state of Asp-B566 enormously, i.e., even a simultaneous forced deprotonation of both Lys-C51 and Arg-C65 does not lead to a protonated Asp-B566.

In this study, the simultaneous deprotonation of both Lys-C51 and ArgC-52, which may mimic the K(C51)S/R(C52)A double mutant (38), results in protonation of Asp-A568 and Glu-C54. Clearly, the protonation of the former is due to the deprotonation of Arg-C52 and the latter to the deprotonation of Lys-C51. No additional changes of protonation pattern are observed compared with the corresponding changes resulting from deprotonation of Lys-C51 or of ArgC-52 alone given in Table 2. This indicates that the influence of the charge state of these residues is essentially localized at their salt bridge partners in contrast to the more delocalized H-bond network discussed above.

Protonation of Asp-B558 at the PsaC/D interface

In our computations for the native PSI complex, all aspartates are ionized except for Asp-B575 and Asp-B558. In particular, Asp-B558 is essentially protonated in native PSI for all cofactor redox states. The protonated state of Asp-B558 relates to a small cavity occupied by the crystal water HOH-22 ($O_{Asp} - O_{water}$ distance of 2.4 Å) (Fig. 1 *B*). Interestingly, the charge state of Asp-B558 changes dramatically from nearly protonated in the native PSI complex (0.97 H^+ at pH 7 with pKa of 8.5 in the $A_{1A}^0A_{1B}^0$ state) to nearly ionized in the P700-F_X core (0.05 H^+ at pH 7 with pKa of 5.7 in the $A_{1A}^0A_{1B}^0$ state). The calculated pKa of 5.7 for Asp-B558 in the P700-F_X core is relatively close to the reference value of 4.0 in aqueous solution. This is evidently due to solvent contacts (Table 1), whereas in the native PSI complex Asp-B558 is subjected to interactions with a network of residues.

Redox potentials of A_1 and F_X in the P700-F_X core

A_1 redox potential

$E_m(A_{1A})$ and $E_m(A_{1B})$ are calculated to be −545 mV and −652 mV, respectively, in the P700-F_X core (Table 3). Although these values are similar to the calculated $E_m(A_1)$ in the native PSI complex ($E_m(A_{1A}) = -531$ mV; $E_m(A_{1B}) = -686$ mV (17)), the shift in $E_m(A_{1B})$ is slightly larger than that in $E_m(A_{1A})$. As a consequence, the asymmetry in the $E_m(A_{1A/B})$ values decreases from 155 mV (17) in the native PSI complex to 107 mV in the P700-F_X core. The decrease in the difference between $E_m(A_{1A})$ and $E_m(A_{1B})$ by 48 mV relative to the native PSI complex can be assigned predominantly to an upshift of 34 mV in $E_m(A_{1B})$ as compared to a downshift of only 14 mV in $E_m(A_{1A})$. In previous work, the direct contributions of the two iron-sulfur clusters F_A/F_B on the $E_m(A_1)$ in the native PSI complex were found to contribute to the downshift nearly symmetrically by 50 mV for $E_m(A_{1A})$ and by 59 mV for $E_m(A_{1B})$ (17). However, the apparent change of the asymmetry for the $E_m(A_{1A/B})$ considering the P700-F_X core could be explained by a small change in protonation probability of Asp-B575. Upon removal of PsaC, the protonation of Asp-B575 remains practically unchanged for reduced A_{1A}^- (0.85 H^+ for the native PSI complex and 0.89 H^+ for the P700-F_X core). But, it increases protonation by 0.1 H^+ for reduced A_{1B}^- (0.17 H^+ for the native PSI complex and 0.27 H^+ for the P700-F_X core). The residue Asp-B575 was proposed to play a crucial role in tuning the $E_m(A_{1A/B})$ values as revealed in the study on the native PSI complex (17). Increasing protonation of this acidic residue stabilizes the reduced state A_1^-, i.e., increases $E_m(A_1)$.

F_X redox potential

From the optical spectrum at room temperature, the shift of $E_m(F_X)$ in urea-treated PSI was measured to be +60mV, where F_A/F_B were removed by chemical dissociation of the subunit PsaC (3). The resulting P700-F_X cores apparently have an increased solvent exposure of F_X and a lack of charge interaction with the F_A and F_B iron-sulfur clusters.

TABLE 3 Rates k^{ET} of ET from A_1 to F_X in P700-F_X core

	Redox potential [mV]		$1/k^{ET}$ [ns]†	
	$E_m(A_1)$	$E_m(F_X)$*	Computation	Experiment
A_{1A}	−545	−628‡	86¶	126**, 180–190††
		−608§	51¶	
A_{1B}	−652	−628‡	7‖	n.d.
		−608§	6‖	n.d.

The corresponding lifetime $1/k^{ET}$ was estimated from the rate expressions, Eqs. (1) and (2), based on the computed redox potentials $E_m(A_1)$ and $E_m(F_X)$.

*Calculated by adding the calculated shift of the $E_m(F_X)$ between the native PSI complex and P700-F_X core (42 mV) to the measured $E_m(F_X)$ in the native PSI complex.

†A_1^- lifetime calculated with reorganization energy $\lambda = 1.0$.

‡Based on the measured $E_m(F_X) = -670$ mV in the native PSI complex (3).

§Based on the measured $E_m(F_X) = -650$ mV in the native PSI complex (43,44).

¶Estimated by Eq. 2.

‖Estimated by Eq. 1.

**(5).

††(9,10).

However, chemical treatment of proteins could conceivably cause modifications and structural rearrangement of the remaining subunits, particularly those near to the PsaA/PsaB interface with PsaC. Nevertheless, simply by using the atomic coordinates of the crystal structure of the native PSI complex for the remaining subunits of the P700-F_X core, the calculated $E_m(F_X)$ is 42 mV more positive than that for the native PSI complex, which is consistent with the experimentally measured shift of 60 mV in $E_m(F_X)$ for urea-treated PSI (3). This implies that possible structural changes in the P700-F_X core that are induced by urea treatment are either small or not significant for the $E_m(F_X)$, which justifies the structural model for the P700-F_X core used in this study.

One may argue that the shift of the $E_m(F_X)$ is due to the removal of the negatively charged groups F_A/F_B by changing from the native PSI complex to the P700-F_X core. To test this idea, we calculated the ''direct contribution'' of different residues/cofactors on $E_m(F_X)$ in the native PSI complex with all titratable groups in standard protonation state at pH 7.0 (i.e., the acidic groups being ionized, basic groups protonated, and His neutral) (Fig. 2). Here, the negatively charged groups F_A and F_B are responsible for downshifts of the $E_m(F_X)$ in the native PSI complex, by 110 mV and 34 mV, respectively. Due to the additivity of the direct contributions, these contributions to the $E_m(F_X)$ yield a total downshift of 144 mV in the native PSI complex. Thus, elimination of atomic charges on both F_A and F_B from the native PSI complex should upshift the $E_m(F_X)$ by 144 mV. However, in the native PSI complex, protein charges in the PsaC, PsaD, and PsaE subunits essentially neutralize the downshift of $E_m(F_X)$ caused by the presence of $F_{A/B}$, with an upshift of 112 mV, contributed predominantly by an upshift of 90 mV from PsaC. Thus, the total direct influence of the charges on PsaC with $F_{A/B}$, PsaD, and PsaE on $E_m(F_X)$ amounts to a downshift of −32 mV only. Note that all these values, especially the influence of $F_{A/B}$ on $E_m(F_X)$, are valid only in the presence of the protein dielectric volumes from PsaC, PsaD, and PsaE whose dielectric constant was set to $\varepsilon_P = 4$.

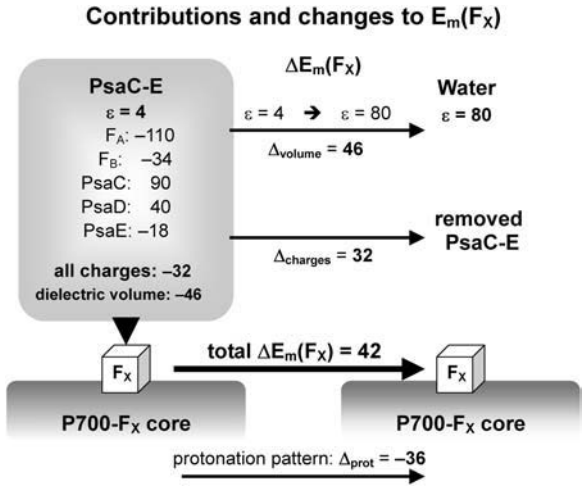

FIGURE 2 Direct influence on the shift of $E_m(F_X)$ from F_A, F_B, and PsaC, PsaD, PsaE (PsaC-E) charges ($\Delta_{charges}$) and from dielectric volume (Δ_{volume}) by changing from the native PSI to the P700-F_X core. Calculated contributions and shifts (Δ) to $E_m(F_X)$ are given in units of mV. Contributions to $E_m(F_X)$ from specific components of the PsaC-E subunits are given in the left box that schematically represents these subunits. Changes (shifts) in $E_m(F_X)$ upon removal of the PsaC-E subunits are denoted by Δ. The total shift is given as the sum of shifts from all charges, volume, and changes in the protonation pattern associated with them, i.e., $\Delta E_m(F_X) = \Delta_{charges} + \Delta_{volume} + \Delta_{prot}$. The direct influence from dielectric volume is obtained if for vanishing charges in the PsaC-E subunits the protein dielectric volume of PsaC-E with $\varepsilon_P = 4$ is removed resulting in water occupancy with $\varepsilon_W = 80$. The indirect influence due to associated changes in the protonation pattern of titratable residues (Δ_{prot}) upon the removal of these subunits and $F_{A/B}$ is given for the charges and the dielectric volume of all three removed subunits.

Removal of the subunits and cofactors from the native PSI complex is also accompanied by exposure of the resulting P700-F_X core to bulk water. This effect is considered in our model by the replacement of the dielectric constant $\varepsilon_P = 4$ by $\varepsilon_W = 80$ in the volume of the removed protein and cofactors. This procedure is accompanied by generation of a new water accessible surface on the remaining PSI-RC scanned by a probe molecule of radius of 1.4 Å. Here, we obtain an upshift of $E_m(F_X)$ by 46 mV due to the replacement of protein dielectric volume by the high dielectric of water in changing from the native PSI complex to a P700-F_X core.

Creation of a new protein surface is often accompanied by a change of protonation pattern of nearby titratable residues. The change of protonation pattern from the native PSI complex to the P700-F_X core, though it is subtle, results in a downshift of $E_m(F_X)$ by 36 mV. Therefore, the total influence on the shift of $E_m(F_X)$ in the P700-F_X core, originating from the replacement of the protein volume of PsaC by water, yields an upshift of only 10 mV with respect to the native PSI complex. Together with the upshift of 32 mV obtained by the removal of the atomic charges from the subunits and of $F_{A/B}$ to generate P700-F_X, $E_m(F_X)$ in the P700-F_X core is by 42 mV higher than that in the native PSI complex.

Although F_X is not embedded in PsaC, the atomic charges of this subunit provide a significant stabilization to F_X^-. Hence, the upshift of the $E_m(F_X)$ caused by PsaC implies that in addition to the negatively charged iron-sulfur clusters F_A and F_B, PsaC is effectively rich in positive charges originating from basic groups. Among the eight basic residues and nine acidic residues in PsaC, the F_X binding niche is particularly rich in basic residues (Lys-C51, Arg-C52, and Arg-C65) rather than acidic residues (Glu-C54). These basic groups simultaneously contribute to the binding with subunits PsaA and PsaB, whose interfaces are rich in negatively charged acidic groups distributed symmetrically about the F_X iron-sulfur cluster (9).

Kinetics of ET from A_1 to F_X in the P700-F_X core

The lifetime ($t_{1/e} = 1/k^{ET}$) of the reduced state A_1^- in PSI is limited by ET processes and exhibits two dominant time

phases. It has been established that ET from A_1 to F_X is biphasic, the slower phase being 206–355 ns and the faster phase being 10–36 ns (11–16,39). Mutational studies of either Trp-A697 or Trp-B673 to Phe near A_{1A}/A_{1B} suggested that the former/latter originates from the forward ET from A_{1A}/A_{1B} to F_X (5,16,40,41). In previous work (17) based on calculated $E_m(A_{1A/B})$, we obtained $t_{1/e} = 220–375$ ns from the E_m difference between A_{1A} and F_X and $t_{1/e} = 6–8$ ns from the E_m difference between A_{1B} and F_X, in agreement with the assignment in the mutant study (16). These estimates for the A_1^- lifetime were obtained by using a reorganization energy of $\lambda = 1.0$ estimated from the kinetics of ET from A_1 to F_X (42).

From kinetic studies with UV-VIS (9) or EPR (10) spectroscopy, it was revealed that the rate for the slow phase of ET from A_{1A} to F_X remained unchanged in urea-treated PSI (characteristic time of 180–190 ns). In a recent kinetic study also on urea-treated PSI by Gong et al. (5), the corresponding ET process was reexamined under the same conditions, giving rise to a slightly accelerated ET with a shorter lifetime of 126 ns.

With the same value of reorganization energy $\lambda = 1.0$ as used for the native PSI complex for ET from A_{1A} to F_X, we calculate lifetimes of 51–86 ns (Table 3) using Eqs. 1 and 2. These lifetimes are moderately shorter than the values computed for the native PSI complex (220–375 ns (17)). Hence, our calculated results show a small acceleration of ET for the P700-F_X core model, consistent with the measurement by Gong et al. for the urea-prepared P700-F_X core (5). The calculated rate for ET from A_{1A} to F_X is slightly larger than the measured rate. To reproduce the corresponding experimental lifetime of 126 ns (5), we can, for instance, increase $E_m(A_{1A})$ by 15 mV (i.e., rendering the ET reaction by 15 mV less exergonic) keeping all other conditions fixed. Such shifts in E_m are smaller than $1\ k_BT = 26$ mV and are therefore within the uncertainty limit of the measured E_m, reorganization energy, or calculated E_m associated with a tiny but possible protein structural change depending on P700-F_X core preparation. Other factors, which we ignore in this study, such as protein dynamics may contribute to the remaining discrepancy, although the mere account of such factors without experimentally established structural-related information may result in additional artifacts. This study suggests that the upshift of $E_m(F_X)$ in the P700-F_X core preparation may be a key to understanding the acceleration of the ET process found for urea-treated PSI by Gong et al. (5).

It was suggested that urea treatment could be accompanied with a partial (10% (2) or 30% (10)) loss of F_X with respect to the native PSI complex. With F_X absent, ET cannot proceed past A_1. Thus, a longer lifetime of the charge-separated state $P_{700}^+ A_1^-$ in P_{700}-F_X core is observed (10). Computationally it is possible to delete PsaC, PsaD, and PsaE from the crystal structure of the native PSI complex. Based on this simple model for the P_{700}-F_X core structure, we can reproduce the measured shift of $E_m(F_X)$ (3) and, as a consequence, obtain an acceleration of ET from A_1 to F_X as observed in the kinetic measurements (5) for urea-treated PSI. Thus, this study demonstrates that this simple model for the P700-F_X core based on the native PSI complex can essentially explain the experimental results. Furthermore, these computational results suggest that the structural essentials of the PsaA/PsaB core of the native PSI complex are conserved in the urea-treated P700-F_X core as previously suggested (2).

SUPPLEMENTARY MATERIAL

An online supplement to this article can be found by visiting BJ Online at http://www.biophysj.org.

We thank Dr. Donald Bashford and Dr. Martin Karplus for providing the programs MEAD and CHARMM22, respectively. We thank Dr. Wolfram Saenger and Dr. Norbert Krauß for useful discussions.

This work was supported by the Deutsche Forschungsgemeinschaft SFB 498, Projects A3 and A5, GRK 80/2, GRK 268, and GKR 788/1, and by the U.S. National Science Foundation (MCB-MCB-0117079). H.I. was supported by the German Academic Exchange Service (DAAD).

REFERENCES

1. Jordan, P., P. Fromme, H. T. Witt, O. Klukas, W. Saenger, and N. Krauß. 2001. Three-dimensional structure of cyanobacterial photosystem I at 2.5 Å resolution. *Nature*. 411:909–917.
2. Golbeck, J. H., K. G. Parrett, T. Mehari, K. L. Jones, and J. J. Brand. 1988. Isolation of the intact photosystem I reaction center core containing P700 and iron-sulfur center F_X. *FEBS Lett*. 228:268–272.
3. Parrett, K. G., T. Mehari, P. G. Warren, and J. H. Golbeck. 1989. Purification and properties of the intact P-700 and F_X-containing photosystem I core protein. *Biochim. Biophys. Acta*. 973:324–332.
4. Golbeck, J. H. 2003. The binding of cofactors to photosystem I analyzed by spectroscopic and mutagenic methods. *Annu. Rev. Biophys. Biomol. Struct*. 32:237–256.
5. Gong, X. M., R. Agalarov, K. Brettel, and C. Carmeli. 2003. Control of electron transport in photosystem I by the iron-sulfur cluster F_X in response to intra- and intersubunit interactions. *J. Biol. Chem*. 278: 19141–19150.
6. Yu, J., L. B. Smart, Y. S. Jung, J. Golbeck, and L. McIntosh. 1995. Absence of PsaC subunit allows assembly of photosystem I core but prevents the binding of PsaD and PsaE in *Synechocystis* sp. PCC6803. *Plant Mol. Biol*. 29:331–342.
7. Shen, G., J. Zhao, S. K. Reimer, M. L. Antonkine, Q. Cai, S. M. Weiland, J. H. Golbeck, and D. A. Bryant. 2002. Assembly of photosystem I. I. Inactivation of the *rubA* gene encoding a membrane-associated rubredoxin in the cyanobacterium *Synechococcus* sp. PCC 7002 causes a loss of photosystem I activity. *J. Biol. Chem*. 277: 20343–20354.
8. Shen, G., M. L. Antonkine, A. van der Est, I. R. Vassiliev, K. Brettel, R. Bittl, S. G. Zech, J. Zhao, D. Stehlik, D. A. Bryant, and J. H. Golbeck. 2002. Assembly of photosystem I. II. Rubredoxin is required for the in vivo assembly of F_X in *Synechococcus* sp. PCC 7002 as shown by optical and EPR spectroscopy. *J. Biol. Chem*. 277:20355–20366.
9. Lüneberg, J., P. Fromme, P. Jekow, and E. Schlodder. 1994. Spectroscopic characterization of PS I core complexes from thermophilic *Synechococcus* sp: identical reoxidation kinetics of A_1^- before and after removal of theiron-sulfur-clusters F_A and F_B. *FEBS Lett*. 338:197–202.

10. van der Est, A., C. Bock, J. Golbeck, K. Brettel, P. Sétif, and D. Stehlik. 1994. Electron transfer from the acceptor A_1 to the iron-sulfur centers in photosystem I as studied by transient EPR spectroscopy. *Biochemistry*. 33:11789–11797.

11. Brettel, K. 1988. Electron transfer from A_1^- to an iron-sulfur center with $t_{1/2}$ = 200 ns at room temperature in photosystem I characterization by flash absorption spectroscopy. *FEBS Lett*. 239: 93–98.

12. Sétif, P., and K. Brettel. 1993. Forward electron transfer from phylloquinone A_1 to iron-sulfur centers in spinach photosystem I. *Biochemistry*. 32:7846–7854.

13. Leibl, W., B. Toupance, and J. Breton. 1995. Photoelectric characterization of forward electron transfer to iron-sulfur centers in photosystem I. *Biochemistry*. 34:10237–10244.

14. Joliot, P., and A. Joliot. 1999. In vivo analysis of the electron transfer within photosystem I: are the two phylloquinones involved? *Biochemistry*. 38:11130–11136.

15. Purton, S., D. R. Stevens, I. P. Muhiuddin, M. C. W. Evans, S. Carter, S. E. J. Rigby, and P. Heathcote. 2001. Site-directed mutagenesis of PsaA residue W693 affects phylloquinone binding and function in the photosystem I reaction center of *Chlamydomonas reinhardtii*. *Biochemistry*. 40:2167–2175.

16. Guergova-Kuras, M., B. Boudreaux, A. Joliot, P. Joliot, and K. Redding. 2001. Evidence for two active branches for electron transfer in photosystem I. *Proc. Natl. Acad. Sci. USA*. 98:4437–4442.

17. Ishikita, H., and E. W. Knapp. 2003. Redox potential of quinones in both electron transfer branches of photosystem I. *J. Biol. Chem.* 278:52002–52011.

18. Antonkine, M. L., P. Jordan, P. Fromme, N. Krauß, J. H. Golbeck, and D. Stehlik. 2003. Assembly of protein subunits within the stromal ridge of photosystem I. Structural changes between unbound and sequentially PS I-bound polypeptides and correlated changes of the magnetic properties of the terminal iron sulfur clusters. *J. Mol. Biol*. 327:671–697.

19. Sakuragi, Y., B. Zybailov, G. Shen, D. A. Bryant, J. H. Golbeck, B. A. Diner, I. Karygina, Y. N. Pushkar, and D. Stehlik. 2005. Recruitment of a foreign quinone into the A_1 site of photosystem I. Characterization of a *menB rubA* double deletion mutant in *Synechococcus* sp. PCC 7002 devoid of F_X, F_A, and F_B and containing plastoquinone or exchanged 9,10-anthraquinone. *J. Biol. Chem.* 280: 12371–12381.

20. Pushkar, Y. N., I. Karyagina, D. Stehlik, S. Brown, and A. van der Est. 2005. Recruitment of a foreign quinone into the A_1 site of photosystem I. Consecutive forward electron transfer from A_0 to A_1 to F_X with anthraquinone in the A_1 site as studied by transient EPR. *J. Biol. Chem.* 280:12382–12390.

21. Li, N., J. Zhao, P. V. Warren, J. T. Warden, D. A. Bryant, and J. H. Golbeck. 1991. PsaD is required for the stable binding of PsaC to the photosystem I core protein of *Synechococcus* sp. PCC 6301. *Biochemistry*. 30:7863–7872.

22. Rodday, S. M., S. S. Jun, and J. Biggins. 1993. Interaction of the F_A/F_B-containing subunit with the photosystem-1 core heterodimer. *Photosynth. Res*. 36:1–9.

23. Brooks, B. R., R. E. Bruccoleri, B. D. Olafson, D. J. States, S. Swaminathan, and M. Karplus. 1983. CHARMM: a program for macromolecular energy minimization and dynamics calculations. *J. Comput. Chem*. 4:187–217.

24. MacKerell, A. D. Jr., D. Bashford, R. L. Bellott, R. L. Dunbrack Jr., J. D. Evanseck, M. J. Field, S. Fischer, J. Gao, H. Guo, S. Ha, D. Joseph-McCarthy, L. Kuchnir, K. Kuczera, F. T. K. Lau, C. Mattos, S. Michnick, T. Ngo, D. T. Nguyen, B. Prodhom, W. E. Reiher III, B. Roux, M. Schlenkrich, J. C. Smith, R. Stote, J. Straub, M. Watanabe, J. Wiorkiewicz-Kuczera, D. Yin, and M. Karplus. 1998. All-atom empirical potential for molecular modeling and dynamics studies of proteins. *J. Phys. Chem. B*. 102:3586–3616.

25. Rabenstein, B., G. M. Ullmann, and E. W. Knapp. 1998. Calculation of protonation patterns in proteins with structural relaxation and molecular ensembles: application to the photosynthetic reaction center. *Eur. Bophys. J*. 27:626–637.

26. Mouesca, J., J. L. Chen, L. Noodleeman, D. Bashford, and D. A. Case. 1994. Density functional/Poisson-Boltzmann calculations of redox potentials for iron-sulfur clusters. *J. Am. Chem. Soc*. 116:11898–11914.

27. Davis, I. H., P. Heathcote, D. J. MacLachlan, and M. C. W. Evance. 1993. Modulation analysis of the electron spin echo signals of in vivo oxidised primary donor ^{14}N chlorophyll centres in bacterial, P870 and P960, and plant Photosystem I, P700, reaction centres. *Biochim. Biophys. Acta*. 1143:183–189.

28. Rigby, S. E. J., J. H. A. Nugent, and P. J. O'Malley. 1994. ENDOR and special triple resonance studies of chlorophyll cation radicals in photosystem 2. *Biochemistry*. 33:10043–10050.

29. Käss, H., and W. Lubitz. 1996. Evaluation of 2D-ESEEM data of ^{15}N-labeled radical cations of the primary donor P_{700} in photosystem I and chlorophyll a. *Chem. Phys. Lett*. 251:193–203.

30. Mac, M., N. R. Bowlby, G. T. Babcock, and J. McCracken. 1998. Monomeric spin density distribution in the primary donor of photosystem I as determined by electron magnetic resonance: functional and thermodynamic implications. *J. Am. Chem. Soc*. 120: 13215–13223.

31. Bashford, D., and M. Karplus. 1990. pKa's of ionizable groups in proteins: atomic detail from a continuum electrostatic model. *Biochemistry*. 29:10219–10225.

32. Rabenstein, B. 1999. Karlsberg online manual. http://agknapp.chemie.fu-berlin.de/karlsberg/.

33. Prince, R. C., P. L. Dutton, and J. M. Bruce. 1983. Electrochemistry of ubiquinones: menaquinones and plastoquinones in aprotic solvents. *FEBS Lett*. 160:273–276.

34. Ishikita, H., and E. W. Knapp. 2005. Energetics of proton transfer pathways in reaction centers from *Rhodobacter sphaeroides*: the Glu-H173 activated mutants. *J. Biol. Chem.* 280:12446–12450.

35. Ishikita, H., and E. W. Knapp. 2005. Redox potential of cytochrome c550 in the cyanobacterium *Thermosynechococcus elongatus*. *FEBS Lett*. 579:3190–3194.

36. Page, C. C., C. C. Moser, X. Chen, and P. L. Dutton. 1999. Natural engineering principles of electron tunnelling in biological oxidation-reduction. *Nature*. 402:47–52.

37. Hastings, G., and V. Sivakumar. 2001. A Fourier transform infrared absorption difference spectrum associated with the reduction of A_1 in photosystem I: are both phylloquinones involved in electron transfer? *Biochemistry*. 40:3681–3689.

38. Fischer, N., P. Sétif, and J. D. Rochaix. 1997. Targeted mutations in the *psaC* gene of *Chlamydomonas reinhardtii*: preferential reduction of F_B at low temperature is not accompanied by altered electron flow from photosystem I to ferredoxin. *Biochemistry*. 36:93–102.

39. Yang, F., G. Shen, W. M. Schluchter, B. L. Zybailov, A. O. Ganago, I. R. Vassiliev, D. A. Bryant, and J. H. Golbeck. 1998. Deletion of the PsaF polypeptide modifies the environment of the redox-active phylloquinone (A_1). Evidence for unidirectionality of electron transfer in photosystem I. *J. Phys. Chem. B*. 102:8288–8299.

40. Xu, W., P. Chitnis, A. Valieva, A. van der Est, Y. N. Pushkar, M. Krzystyniak, C. Teutloff, S. G. Zech, R. Bittl, D. Stehlik, B. Zybailov, G. Shen, and J. H. Golbeck. 2003. Electron transfer in cyanobacterial photosystem I: I. Physiological and spectroscopic characterization of site-directed mutants in a putative electron transfer pathway from A_0 through A_1 to F_X. *J. Biol. Chem.* 278:27864–27875.

41. Xu, W., P. R. Chitnis, A. Valieva, A. van der Est, K. Brettel, M. Guergova-Kuras, Y. N. Pushkar, S. G. Zech, D. Stehlik, G. Shen, B. Zybailov, and J. H. Golbeck. 2003. Electron transfer in cyanobacterial photosystem I: II. Determination of forward electron transfer rates of site-directed mutants in a putative electron transfer pathway from A_0 through A_1 to F_X. *J. Biol. Chem.* 278:27876–27887.

42. Schlodder, E., K. Falkenberg, M. Gergeleit, and K. Brettel. 1998. Temperature dependence of forward and reverse electron transfer from A_1^-, the reduced secondary electron acceptor in photosystem I. *Biochemistry*. 37:9466–9476.

43. Shinkarev, V., I. Vassiliev, and J. H. Golbeck. 2000. A kinetic assessment of the sequence of electron transfer from F_X to F_A and further to F_B in photosystem I: the value of the equilibrium constant between F_X and F_A. *Biophys. J.* 78:363–372.

44. Semenov, A. Y., I. R. Vassiliev, A. van der Est, M. D. Mamedov, B. Zybailov, G. Shen, D. Stehlik, B. A. Diner, P. R. Chitnis, and J. H. Golbeck. 2000. Recruitment of a foreign quinone into the A_1 site of photosystem I. *J. Biol. Chem.* 275:23429–23438.